LONG-TERM PROPAGATION OF HIGH AREA-TO-MASS RATIO OBJECTS USING AVERAGED EQUATIONS

A. J. Rosengren and D. J. Scheeres

University of Colorado at Boulder, 429 UCB, Boulder, CO, 80309, USA,
Email: {aaron.rosengren, scheeres}@colorado.edu

ABSTRACT

The discovery of high area-to-mass ratio (HAMR) debris in near geosynchronous orbit (GEO) raises concern for the sustainability of this unique resource. It is thought that HAMR objects are sheets of multilayer insulation detaching from satellites in GEO disposal orbits due to material degradation. Such objects are subject to gravitational perturbations due to the Earth's oblateness and the Moon and Sun, as well as the effects of solar radiation pressure (SRP). We have developed a first-order averaged model, explicitly given in terms of the Milankovitch elements, which provides a very accurate description of the long-term orbit behavior and allows for a qualitative understanding. We present this model and discuss its fundamental predictions, including the Saros resonance and the systematic structure of the inclination-node phase space. We also extend the model's domain of validity by incorporating the parallactic term into the third-body disturbing function expansion and the Earth's shadow for SRP.

Key words: high area-to-mass ratio objects; averaging; orbit perturbations; Milankovitch orbital elements.

1. INTRODUCTION

The long-term dynamics of high area-to-mass ratio (HAMR) objects has been studied extensively since the discovery of this debris population in near GEO orbits [3, 7]. Most studies concentrate on numerical integration of the precise set of differential equations, which can give an accurate trajectory of a particular object, but not necessarily general insight into the important aspects of the governing laws. Our purpose, however, is to adopt the simplest possible expressions useful for studying the long-term orbital evolution of HAMR debris. These expressions must reveal the qualitative regularities of motion, and they must provide a way of obtaining quantitative predictions of long-term changes. Among the more predominant perturbations acting on HAMR objects are solar radiation pressure (SRP), Earth's oblateness, and third-body gravitational interactions induced by the Sun and the Moon. We have developed a first-order averaged model, based on the Milankovitch formulation of secular

perturbation theory, which accounts for these perturbations and is written in a concise analytical vector form [5, 6]. The secular equations do not depend on expansions in eccentricity or inclination and avoid the small numerical divisors. The disturbing function includes the cannonball model of SRP, the dominant zonal harmonic in the harmonic expansion of Earth's gravitational potential, and the lowest-order term in the Legendre expansion of the lunar and solar disturbing functions (i.e., Hill's approximation). Under these approximations, the semi-major axis, a, does not undergo any secular changes and the problem reduces to understanding the remaining four orbital elements, e, i, Ω, and ω, at a given semi-major axis. Higher harmonics in the lunar disturbing function may become important for HAMR objects in highly-eccentric GEO orbits, and their neglect sets an upper limit to the size of orbit for which the analysis is applicable [4]. On the other hand, neglect of higher harmonics in Earth's gravitational field and Earth's shadow effects for SRP sets a lower limit to the orbital radius.

Using this model, we study the dynamics of HAMR objects, and explore the various resonance effects caused by the complex coupling between the Earth-Moon-Sun system and the predominate perturbations. We discuss a unique systematic structure associated with their distribution in inclination and ascending node phase space, and investigate the extent to which the qualitative properties of the orbit persist with increasing area-to-mass. We then extend the domain of validity of this model by incorporating the parallactic term into the disturbing function expansion and the Earth's shadow effects for SRP acceleration. All notations in this article are the same as in [6] and all symbols have their conventional significance.

2. MILANKOVITCH ORBITAL ELEMENTS

The first-order perturbation theory can be formulated simply and elegantly in terms of the Milankovitch elements–the two vectorial integrals of the unperturbed two-body problem [5, 6]. The angular momentum vector, $\boldsymbol{H} = \sqrt{\mu a(1 - e^2)}\hat{\boldsymbol{h}}$, and eccentricity vector, $\boldsymbol{e} = e\hat{\boldsymbol{e}}$, describe the spatial orientation, geometrical shape, and size of the osculating orbit, and, together with the scalar integral that represents the motion in time, constitutes

a complete set of orbital elements. Geometrically, $\boldsymbol{H}$ points perpendicular to the instantaneous orbit plane and $\boldsymbol{e}$ points towards the instantaneous periapsis. Their secular perturbations equations in Gaussian form, for an arbitrary disturbing acceleration $\boldsymbol{a}_d$, can be stated as [5]

$$\dot{\boldsymbol{H}} = \frac{1}{T} \oint \widetilde{\boldsymbol{r}} \cdot \boldsymbol{a}_d \, \mathrm{d}t \tag{1}$$

$$\dot{\boldsymbol{e}} = \frac{1}{T} \oint \frac{1}{\mu} \left(\widetilde{\boldsymbol{v}} \cdot \widetilde{\boldsymbol{r}} - \widetilde{\boldsymbol{H}} \right) \cdot \boldsymbol{a}_d \, \mathrm{d}t \tag{2}$$

where T is the period of the orbit.

When the perturbations come from a potential, the semi-major axis, a, does not undergo any secular changes and hence $\boldsymbol{H}$ can be scaled by $\sqrt{\mu a}$. For this vector, denoted here as $\boldsymbol{h}$, together with $\boldsymbol{e}$, the secular Milankovitch equations take a compact and symmetrical form

$$\dot{\boldsymbol{h}} = \widetilde{\boldsymbol{h}} \cdot \left(\frac{\partial \mathcal{R}^*}{\partial \boldsymbol{h}} \right)^T + \widetilde{\boldsymbol{e}} \cdot \left(\frac{\partial \mathcal{R}^*}{\partial \boldsymbol{e}} \right)^T \tag{3}$$

$$\dot{\boldsymbol{e}} = \widetilde{\boldsymbol{e}} \cdot \left(\frac{\partial \mathcal{R}^*}{\partial \boldsymbol{h}} \right)^T + \widetilde{\boldsymbol{h}} \cdot \left(\frac{\partial \mathcal{R}^*}{\partial \boldsymbol{e}} \right)^T \tag{4}$$

where $\mathcal{R}^* = \mathcal{R}(\boldsymbol{h}, \boldsymbol{e})/\sqrt{\mu a}$. The average potential is

$$\mathcal{R}(\boldsymbol{h}, \boldsymbol{e}) = \frac{1}{2\pi} \int_0^{2\pi} \mathcal{R}(\boldsymbol{\alpha}, M) \, \mathrm{d}M \tag{5}$$

where $\boldsymbol{\alpha}$ is an arbitrary set of orbital elements excluding the mean anomaly, M. Note that physically meaningful solutions are restricted to the four-dimensional manifold on which $\boldsymbol{h} \cdot \boldsymbol{e} = 0$ and $\boldsymbol{h} \cdot \boldsymbol{h} + \boldsymbol{e} \cdot \boldsymbol{e} = 1$.

3. AVERAGED EQUATIONS OF MOTION

In terms of the Milankovitch elements, the first-order averaged equations for SRP, J_2, and lunisolar perturbations take the form [6]

$$\dot{\boldsymbol{h}} = \dot{\boldsymbol{h}}_{srp} + \dot{\boldsymbol{h}}_{20} + \dot{\boldsymbol{h}}_s + \dot{\boldsymbol{h}}_m \tag{6}$$

$$\dot{\boldsymbol{e}} = \dot{\boldsymbol{e}}_{srp} + \dot{\boldsymbol{e}}_{20} + \dot{\boldsymbol{e}}_s + \dot{\boldsymbol{e}}_m \tag{7}$$

where the averaged SRP dynamics are given by

$$\dot{\boldsymbol{h}}_{srp} = -\frac{3}{2} \sqrt{\frac{a}{\mu}} \frac{\beta}{d_s^2} \widetilde{\hat{\boldsymbol{d}}}_s \cdot \boldsymbol{e} \tag{8}$$

$$\dot{\boldsymbol{e}}_{srp} = -\frac{3}{2} \sqrt{\frac{a}{\mu}} \frac{\beta}{d_s^2} \widetilde{\hat{\boldsymbol{d}}}_s \cdot \boldsymbol{h} \tag{9}$$

in which $\beta = (1 + \rho)(A/m)P_\Phi$, ρ is the reflectance, A/m is the appropriate cross-sectional area-to-mass ratio in m^2/kg, P_Φ is the solar radiation constant ($\approx 1 \times 10^8$ kg km^3/s^2/m^2), and $\boldsymbol{d}_s = d_s \hat{\boldsymbol{d}}_s$ is the vector from the Earth to the Sun. The secular Milankovitch equations resulting from the oblateness of the Earth can be stated as

$$\dot{\boldsymbol{h}}_{20} = \frac{3nC_{20}}{2a^2 h^5} (\hat{\boldsymbol{p}} \cdot \boldsymbol{h}) \widetilde{\hat{\boldsymbol{p}}} \cdot \boldsymbol{h} \tag{10}$$

$$\dot{\boldsymbol{e}}_{20} = \frac{3nC_{20}}{4a^2 h^5} \left\{ \left[1 - \frac{5}{h^2} (\hat{\boldsymbol{p}} \cdot \boldsymbol{h})^2 \right] \widetilde{\boldsymbol{h}} + 2(\hat{\boldsymbol{p}} \cdot \boldsymbol{h}) \widetilde{\hat{\boldsymbol{p}}} \right\} \cdot \boldsymbol{e} \tag{11}$$

where $C_{20} = -J_2 R^2$ is the oblateness gravity field coefficient, R is the mean equatorial radius of Earth, n is the mean motion, and $\hat{\boldsymbol{p}}$ is aligned with Earth's rotation pole. The Hill-approximated third-body dynamics resulting from a body with gravitational parameter μ_p are

$$\dot{\boldsymbol{h}}_p = \frac{3\mu_p}{2nd_p^3} \hat{\boldsymbol{d}}_p \cdot (5\boldsymbol{ee} - \boldsymbol{hh}) \cdot \widetilde{\hat{\boldsymbol{d}}}_p \tag{12}$$

$$\dot{\boldsymbol{e}}_p = \frac{3\mu_p}{2nd_p^3} \left[\hat{\boldsymbol{d}}_p \cdot (5\boldsymbol{eh} - \boldsymbol{he}) \cdot \widetilde{\hat{\boldsymbol{d}}}_p - 2\widetilde{\boldsymbol{h}} \cdot \boldsymbol{e} \right] \tag{13}$$

in which where $\boldsymbol{d}_p$ is the position vector of the perturbing body. The product of two vectors, $\boldsymbol{ab}$, is called a dyad and is equivalent to the outer product (i.e., $[\boldsymbol{a}][\boldsymbol{b}]^T$).

4. LONG-TERM BEHAVIOR OF GEO ORBITS

Nearly fifty years have elapsed since satellites were first launched into geostationary (equatorial, circular-synchronous) Earth orbit. The motion of uncontrolled GEO satellites is governed by gravitational perturbations. By itself, Earth's oblateness causes the pole of the orbital plane to precess around the pole of Earth's equator, the rate of rotation being proportional to nC_{20}/a^2. Lunisolar perturbations will have a similar effect, but the precession will now take place about the poles of the orbital planes of the Moon and the Sun, respectively, at a rate proportional to n_p^2/n, where n_p is the mean motion of the perturbing body. The motion of the orbit pole of the satellite is a combination of simultaneous precession about these three different axes, one of which, the pole of the Moon's orbit, regresses around the pole of the ecliptic with a period of 18.61 years (i.e., the Saros) [2]. As shown in Fig. 1, uncontrolled GEO satellites precess about the axis of a mean reference plane (the Laplace plane) with a period of nearly 54 years and a corresponding variation in their orbital inclinations of $\pm 15°$. This and all subsequent plots are reported in the Earth-equatorial frame. Note that the inclinations and ascending nodes are strongly correlated.
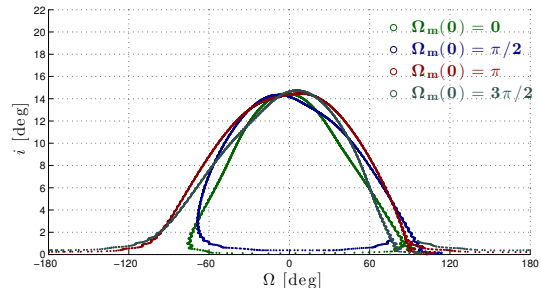

Figure 1. Scatter plot of the time-series, over 54 years, of the orbital plane of initially geostationary objects as predicted by our averaged model for four different initial lunar node positions, i.e., four different launch dates. There is a near-commensurability of the period of the lunar precession and the period of the motion of the satellite's orbital plane.

5. LONG-TERM ORBITAL EVOLUTION OF HAMR OBJECTS

For a given semi-major axis and effective area-to-mass ratio, we define the SRP perturbation angle as

$$\tan \Lambda = \frac{3\beta}{2} \sqrt{\frac{a}{\mu}} \frac{1}{H_e} \tag{14}$$

where H_e is the specific angular momentum of the Earth about the Sun. This angle can be used to rigorously characterize the strength of the SRP perturbation acting on a body as a function of its orbit, its non-gravitational parameter, and the orbit of the Earth about the Sun [5, 6]

The evolution of several HAMR objects released from GEO, obtained using numerical integrations of the averaged equations of motion, are shown in Figs. 2 and 3. We refer the reader to [5] for a complete description of the first- order effects of each perturbing force on the system.
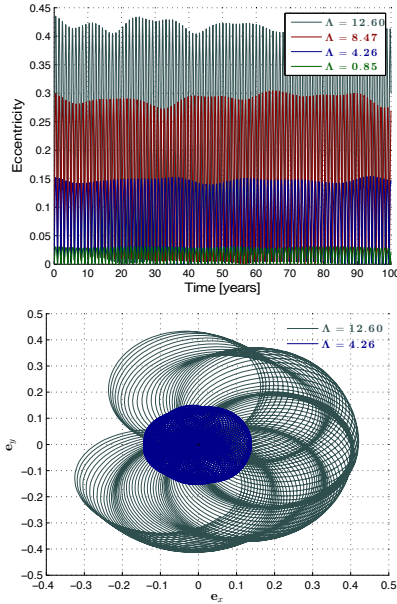
Figure 2. Long-term evolution of the eccentricity and eccentricity vector for different values of Λ.

Saros Resonance and (i, Ω) Phase Space : When the nodal rate of the perturbed system is near-commensurate with the nodal rate of the Moon (i.e., the Saros), the perturbations build up more effectively over long periods to produce significant resonant effects on the orbit. This resonant behavior explains the long-term beating phenomenon that occurs for $\Lambda = 12.60°$ (vide Fig. 3). Fig. 4 shows the time-series of inclination and node for a range of SRP perturbation angles. For $\Lambda = 13.81°$, the nodal period in the equatorial frame is ~18.61 years, thereby inducing a $1\!:\!1$ resonance with the Saros. The qualitative picture of the evolution changes drastically based on the initial lunar node. The pattern associated with their distribution in (i, Ω) phase space is systematic, which means that HAMR objects evolve in predictable ways.
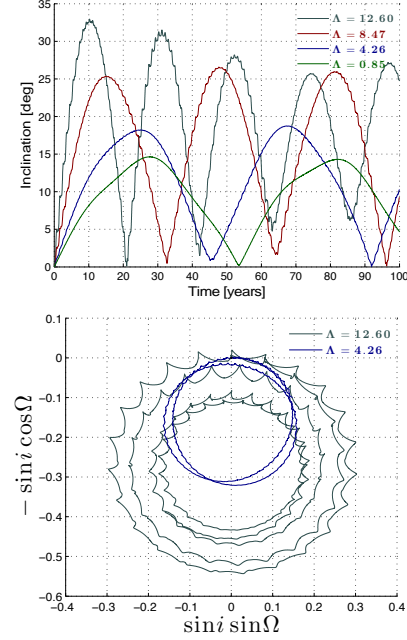
Figure 3. Long-term evolution of the inclination and angular momentum unit vector for different values of Λ.

(a) $\Lambda = 0.85°$

(b) $\Lambda = 4.26°$

(c) $\Lambda = 8.47°$

(d) $\Lambda = 13.81°$ (resonant case)

(e) $\Lambda = 16.59°$
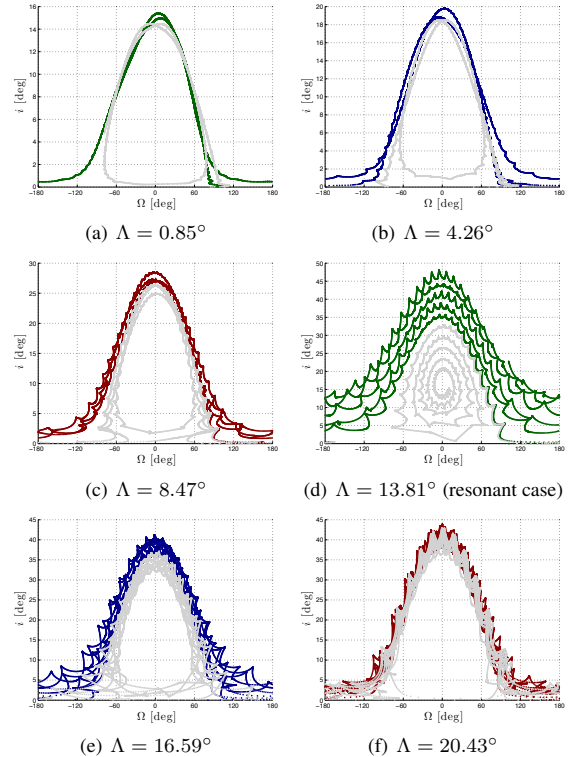
(f) $\Lambda = 20.43°$

Figure 4. Scatter plot of the time-series, over 100 years, of inclination and ascending node, for two different initial lunar node positions for each value of Λ.

6. DISCUSSION

6.1. Accuracy of Averaged Equations

The dynamic behavior underlined by our model is in good agreement, both qualitatively and quantitatively, with the precise numerical integrations of Anselmo and Pardini [3]. We attribute any quantitative differences to our use of the Hill approximation for lunar perturbations and our neglect of Earth shadow effects. Though neither of these secondary perturbations had any significant long-term effects, they can easily be included into our framework.

The Third Harmonic : The perturbation potential resulting from the third harmonics (parallactic term) is

$$\mathcal{R}_{p,3} = \frac{\mu_p}{2d_p^4}\left[5(\boldsymbol{r}\cdot\hat{\boldsymbol{d}}_p)^3 - 3r^2(\boldsymbol{r}\cdot\hat{\boldsymbol{d}}_p)\right] \quad (15)$$

Averaging Eq. 15 over the mean anomaly of the orbiter, computing its partials, and substituting them into Eqs. 3 and 4, the secular equations can be stated as

$$\dot{\boldsymbol{h}}_{p,3} = -\frac{15a\mu_p}{16nd_p^4}\left\{5\left[7(\hat{\boldsymbol{d}}_p\cdot\boldsymbol{e})^2 - (\hat{\boldsymbol{d}}_p\cdot\boldsymbol{h})^2\right]\boldsymbol{e}\right.$$
$$\left. - 10(\hat{\boldsymbol{d}}_p\cdot\boldsymbol{e})(\hat{\boldsymbol{d}}_p\cdot\boldsymbol{h})\boldsymbol{h} + (1-8e^2)\boldsymbol{e}\right\}\cdot\tilde{\hat{\boldsymbol{d}}}_p$$
$$(16)$$

$$\dot{\boldsymbol{e}}_{p,3} = -\frac{15a\mu_p}{16nd_p^4}\left[\left\{5\left[7(\hat{\boldsymbol{d}}_p\cdot\boldsymbol{e})^2 - (\hat{\boldsymbol{d}}_p\cdot\boldsymbol{h})^2\right]\boldsymbol{h}\right.\right.$$
$$\left. - 10(\hat{\boldsymbol{d}}_p\cdot\boldsymbol{e})(\hat{\boldsymbol{d}}_p\cdot\boldsymbol{h})\boldsymbol{e} + (1-8e^2)\boldsymbol{h}\right\}\cdot\tilde{\hat{\boldsymbol{d}}}_p$$
$$\left. - 16(\hat{\boldsymbol{d}}_p\cdot\boldsymbol{e})\tilde{\boldsymbol{h}}\cdot\boldsymbol{e}\right] \quad (17)$$

SRP with Earth Shadow Effects : Using E as the independent variable with E_1 and E_2 being the shadow exit and entry points, the first-order perturbations can be derived in closed form as [1]

$$\dot{\boldsymbol{H}}_{srp} = \frac{a\beta}{2\pi d_s^2}\left\{\left[\frac{3}{2}eE - (1+e^2)\sin E + \frac{1}{4}e\sin 2E\right]\Big|_{E_1}^{E_2}\right.$$
$$\left. \tilde{\hat{\boldsymbol{e}}}\cdot\hat{\boldsymbol{d}}_s + h\left(\cos E - \frac{1}{4}e\cos 2E\right)\Big|_{E_1}^{E_2}\tilde{\hat{\boldsymbol{e}}}_\perp\cdot\hat{\boldsymbol{d}}_s\right\}$$
$$(18)$$

$$\dot{\boldsymbol{e}}_{srp} = \frac{1}{2\pi}\sqrt{\frac{a}{\mu}}\frac{\beta}{d_s^2}\left[\left(e\cos E - \frac{1}{4}\cos 2E\right)\Big|_{E_1}^{E_2}\tilde{\hat{\boldsymbol{e}}}\cdot\tilde{\hat{\boldsymbol{e}}}\right.$$
$$+ h\left(\frac{3}{2}E - e\sin E - \frac{1}{4}\sin 2E\right)\Big|_{E_1}^{E_2}\tilde{\hat{\boldsymbol{e}}}\cdot\tilde{\hat{\boldsymbol{e}}}_\perp$$
$$- h\left(\frac{3}{2}E - 2e\sin E + \frac{1}{4}\sin 2E\right)\Big|_{E_1}^{E_2}\tilde{\hat{\boldsymbol{e}}}_\perp\cdot\tilde{\hat{\boldsymbol{e}}}$$
$$+ h^2\left(\frac{1}{4}\cos 2E\right)\Big|_{E_1}^{E_2}\tilde{\hat{\boldsymbol{e}}}_\perp\cdot\tilde{\hat{\boldsymbol{e}}}_\perp\right]\cdot\hat{\boldsymbol{d}}_s \quad (19)$$

where $h = \sqrt{1-e^2}$, and $\hat{\boldsymbol{e}}_\perp = \tilde{\hat{\boldsymbol{h}}}\cdot\hat{\boldsymbol{e}}$.

6.2. Systematic Structure in (i,Ω) Phase Space

The distribution in (i,Ω) phase space for HAMR objects is the same systematic structure that the uncontrolled GEO satellite population exhibits. For inactive satellites, the oblateness of the Earth and the gravitational pull from the Moon and the Sun force their orbital planes to precess around the Laplace plane (vide Fig. 1). On the Laplace plane, the secular orbital evolution driven by the combined effects of these perturbations is zero, so that the orbits are frozen. This structure for HAMR orbits implies that the classical Laplace plane can be generalized to accommodate SRP, which is a topic of future research.

7. CONCLUSIONS

We presented a complete non-singular formulation of first-order averaging based on the Milankovitch elements. This model accurately captures the long-term orbit behavior, and allows for the general nature of their evolution to be understood. We identified the Saros secular resonance and a systematic (i,Ω) phase space structure. Future work will investigate more realistic SRP models.

ACKNOWLEDGMENTS

REFERENCES

1. Allan, R.R. (1962). Satellite Orbit Perturbations due to Radiation Pressure and Luni-solar Forces. *Q. J. Mech. Appl. Math.*. **15**(3), 283-301.

2. Allan, R.R., and Cook, G.E.. (1964). The long-period motion of the plane of a distant circular orbit. *Proc. R. Soc. Lond. A*. **280**, 97-109.

3. Anselmo, L. & Pardini, C. (2010). Long-term dynamical evolution of high area-to-mass ratio debris released into high earth Orbits. *Acta Astronaut.*. **67**: 204-216.

4. Lidov, M.L. (1962). The Evolution of Orbits of Artificial Satellites of Planets Under the Action of Gravitational Perturbations of External Bodies. *Planet. Space Sci.*. **9**, 719-759.

5. Rosengren, A.J. & Scheeres, D.J. (2013). On the Milankovitch Orbital Elements for Perturbed Keplerian Motion. Submitted to *Celest. Mech. Dyn. Astron.*.

6. Rosengren, A.J. & Scheeres, D.J. (2013). Long-term Dynamics of High Area-to-mass Ratio Objects in High-Earth Orbit. Submitted to *Adv. Space Res.*.

7. Schildknecht, T. et al. (2004). Optical observations of space debris in GEO and in highly-eccentric orbits. *Adv. Space Res.*. **34**, 901-911.